Journal of Materials Chemistry A

Accepted Manuscript

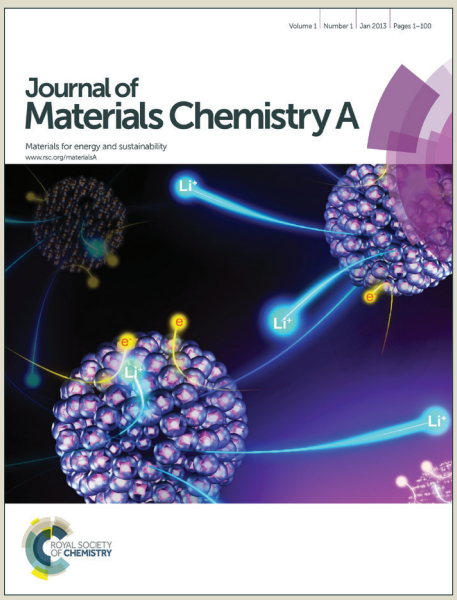

ROYAL SOCIETY OF CHEMISTRY

www.rsc.org/materialsA

Journal of Materials Chemistry A

ARTICLE

Three-dimensional molecular donors combined with polymeric acceptors for high performance fullerene-free organic photovoltaics

Received 00th January 20xx,
Accepted 00th January 20xx

DOI: 10.1039/x0xx00000x

www.rsc.org/

Shi-Yong Liu,[abc] Jae Woong Jung,[a] Chang-Zhi Li,[ab] Jiang Huang,[ad] Jianyuan Zhang,[a] Hongzheng Chen*[b] and Alex K.-Y. Jen*[ab]

The non-fullerene acceptors based organic photovoltaics (OPVs) reported so far are inferior to those derived from fullerenes. This intrigues the speculation whether donors need to be tailored for advancing non-fullerene OPVs. We explored herein two direct arylation-derived diketopyrrolopyrrole(DPP)-based three-dimensional (3D) donors that can deliver respectable power conversion efficiencies (PCEs) of 4.64% and 4.02% with polymeric acceptor N2200 blends, surpassing those obtained from $PC_{71}BM$ (3.56% and 3.22%, respectively). It is found that these 3D-shaped molecular donors can yield the improved photo-to-current conversion and balanced charge transport when blending with linear N2200 polymer. This finding suggests that the engineering molecular geometry can be a promising approach for developing high-performance materials.

1 Introduction

Organic electron donor (D) and acceptor (A) based bulk heterojunction (BHJ) photovoltaics have attracted extensive attentions in the past decade due to their light-weight, good flexibility, and cost-effectiveness merits that can be potentially realized through simple solution processing.[1] Ideally, these electron donors and acceptors should possess intensive and complementary absorption for efficient light harvesting, and the ability to form nano-structured interpenetrating networks of D-A phases for efficient photon-charge generation and transport. Although fullerene derivatives have been widely used as efficient electron acceptor for the BHJ OPVs, they inherit certain drawbacks from pristine fullerene such as weak visible light absorption, limited electronic tunability, and high production cost. Therefore, vigorous efforts have been devoted to developing efficient non-fullerene acceptors,[2] leading to encouraging performance for non-fullerene based OPVs.[3, 4]

Usually, the development of non-fullerene based devices is focused on pairing acceptors with well-established efficient donors. Materials with non-planar and/or 3D architectures in general exhibit better performance in devices than the planar ones,[4-23] which coincides with the spherical feature of fullerenes facilitating multi-directional charge-transport in OPVs.[24] Among numerous non-fullerene acceptors that have been developed so far, their device performance are usually lower than those derived from fullerenes using the same donors.[3,4b,5-22] This intrigued the speculation whether the donors previously developed for blending with fullerenes are suitable for non-fullerene OPV. It inspires us to explore possible strategies on making new donors for better pairing with efficient electron acceptors.

In this paper, four DPP electron-donating units are installed onto either a tetraphenyl-methane or a tetraphenyl-silane core via an atom efficient direct arylation reaction to result in two novel 3D-shaped donor molecules (named as **C-DPP** and **Si-DPP**, Fig. 1). These donors are expected to transport hole carriers in multiple directions in devices.[24] To verify our design concept, two well-known electron acceptors, polymer N2200[25,26] and $PC_{71}BM$ were chosen to pair with 3D-DPP donors (hereafter, 3D-DPPs refers to both **C-DPP** and **Si-DPP**) for solution-processed BHJ OPV devices. The PCEs achieved for **C-DPP**:N2200 and **Si-DPP**:N2200 devices are 4.64 and 4.02%, respectively. In a parallel study, the performance of the devices made from these two molecular donors with $PC_{71}BM$, **C-DPP**:**$PC_{71}BM$** and **Si-DPP**:**$PC_{71}BM$** have lower PCE with 3.56% and 3.22%, respectively. The higher performance derived from the 3D-DPPs:N2200 devices are attributed to the improved incident photon-to-current conversion efficiency (IPCE) from the complementary and broader light absorption of 3D-DPPs:N2200 blends, and the more balanced charge mobility. The PCE of 4.64% is a respectable value for the non-fullerene OPVs using molecular donor and polymer acceptor.[26a-c,27] The current system also

[a] Department of Materials Science and Engineering, University of Washington, Box 352120, Seattle, Washington 98195, USA.E-mail: ajen@u.washington.edu
[b] Department of Polymer Science & Engineering, Zhejiang University, Hangzhou, 310027, P. R. China. E-mail: hzchen@zju.edu.cn
[c] Department of Pharmacy & Chemistry, Taizhou University, Taizhou, 317000, P. R. China
[d] School of Optoelectronic Information, University of Electronic Science and Technology of China, Chengdu 610054, P. R. China

†Electronic Supplementary Information (ESI) available: The detailed synthetic routes of all precursors, ^{1}H NMR spectra of precursors, ^{1}H and ^{13}C NMR, and MALDI-TOF MS spectra of the target 3D-DPPs, and other spectra mentioned in the main text. See DOI: 10.1039/x0xx00000x

represents one of the most efficient BHJs composed of organic semiconductors obtained via direct arylation.[28, 29]

2 Results and discussion

2.1 Synthesis, characterization and theoretical calculation

Fig. 1 depicts the synthetic route of **C-DPP** and **Si-DPP**, and the chemical structure of polymer N2200. An effective strategy to access multi-DPPs[29] was used to install four DPP units onto tetraphenyl-silane and tetraphenyl-methane cores via a ligand-free palladium-catalyzed direct arylation reaction to afford **C-DPP** and **Si-DPP** with excellent yields (90% and 94%, respectively). The n-type polymer N2200 employed in this work (M_n= 49.2kDa, M_w= 89.5 kDa and PDI=1.8) was synthesized by using a modified reported procedure.[25a] The target 3D-DPPs have been fully characterized by ^{1}H and ^{13}C NMR, matrix-assisted laser desorption ionization time of flight (MALDI-TOF) mass spectroscopy (MS) (Fig. S1-S5, see Electronic Supplementary Information (ESI)) and elemental analysis.

Differential scanning calorimetry (DSC) measurement was used to gain insight of intermolecular interactions and crystallinity for **C-DPP** and **Si-DPP**. The DSC scanning from 5 to 280 °C did not find any melting or recrystallization peak (Fig. S6), suggesting both 3D-DPPs are non-crystalline in nature, which is similar to the 3D tetra-PDI previously reported.[22]

Density functional theory (DFT) calculation was carried out to study the molecular geometries of 3D-DPPs. The DFT-optimized geometries show that four DPP units of 3D-DPPs are tetrahedrally orientated with radii of 2.02 and 2.05 nm respectively (Fig. 1), owing to the sp^3 hybrid of C and Si atom centers. Such a tetrahedral architecture should help suppress the tight packing of molecules.[30] Structurally, the four DPP arms are connected via sp^3 C and Si centers. Although the DPP arms have less molecular orbital (MO) overlap between each others, they are close to each other in space at atomic scale. We speculate that the charges on 3D-DPPs would delocalize throughout the DPP arms, and can hop among each other. In this way, 3D distribution and transport of charges will lead to statistically better D-A charge separation and collection.

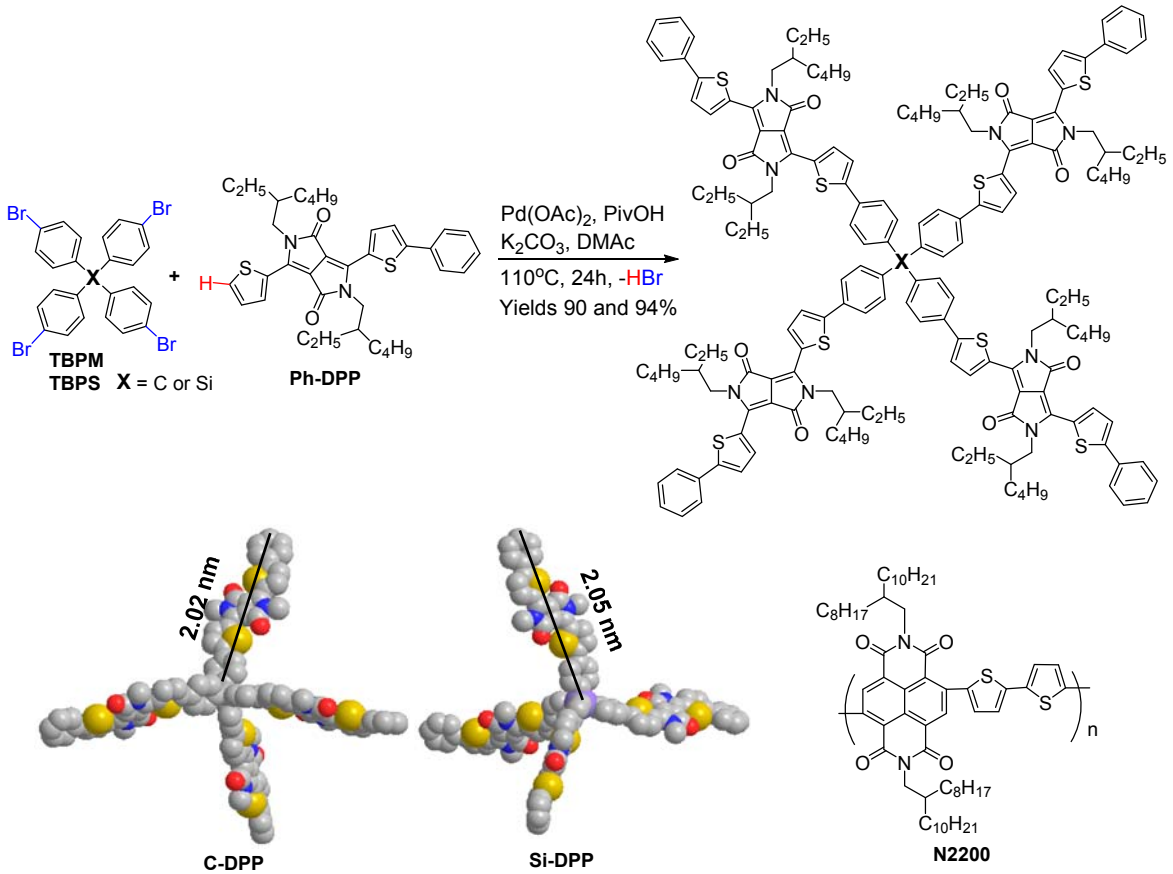

Fig. 1 Direct arylation synthesis of C-DPP and Si-DPP, and their corresponding DFT optimized geometries (ethyl-hexyl chains replaced by methyl groups) shown by space filling models, and the structure of N2200.

2.2 Optical and electrochemical properties

Fig. 2a shows the normalized individual UV-vis absorption spectra of the donors (**C-DPP** and **Si-DPP**), and the acceptor polymer N2200 from spin-coated films. **C-DPP** and **Si-DPP** films exhibit similar absorption spectra, with two peaks at 586 and 640 nm (**C-DPP**) and 582 and 640 nm (**Si-DPP**). These peaks are red-shifted compared to their solution absorption spectra (Fig. S7). In order to maximize light harvesting of BHJs, low bandgap acceptor, N2200 with strong absorption peaks around 400 and 704 nm was chosen to complement the absorption of **C-DPP** and **Si-DPP** donors (Fig. 1a and 2b). Consequently, the blend films composed of 3D-DPPs and N2200 exhibit a strong absorption band ranged from 550 to 750 nm. In contrast to 3D-DPPs:N2200, the 3D-DPPs:$PC_{71}BM$ blends show mainly the 3D-DPPs absorption features with a narrower band from 586 to 640 nm, along with the intense absorption less than 350 nm arising from $PC_{71}BM$(Fig. S8, see ESI).

Besides complementary light absorption of the blends, suitable energetic levels with sufficient frontier orbital energy (FOE) gap between donor and acceptor is also important in driving photon-generated charge dissociation and thus determining the performance of BHJ OPVs. The electrochemical properties of **C-DPP**, **Si-DPP**, N2200, and $PC_{71}BM$ were evaluated by cyclic voltammetry (CV) in CH_2Cl_2 solution. The lowest unoccupied molecular orbital (LUMO) and the highest occupied molecular orbital (HOMO) are estimated from the $E_{1/2}$ values in solution, using the value of -5.1 eV for Fc/Fc^+.[31] Fig. 2c shows the FOEs of the donors and acceptors studied in this work. The bandgap of **C-DPP**, **Si-DPP**, N2200, and $PC_{71}BM$ are 2.01, 2.04, 1.61 and 2.03 eV, respectively. The LUMO of N2200 (-4.11 eV) is close to that of $PC_{71}BM$ (-4.02 eV), indicating N2200 may have comparable electron affinity with $PC_{71}BM$.

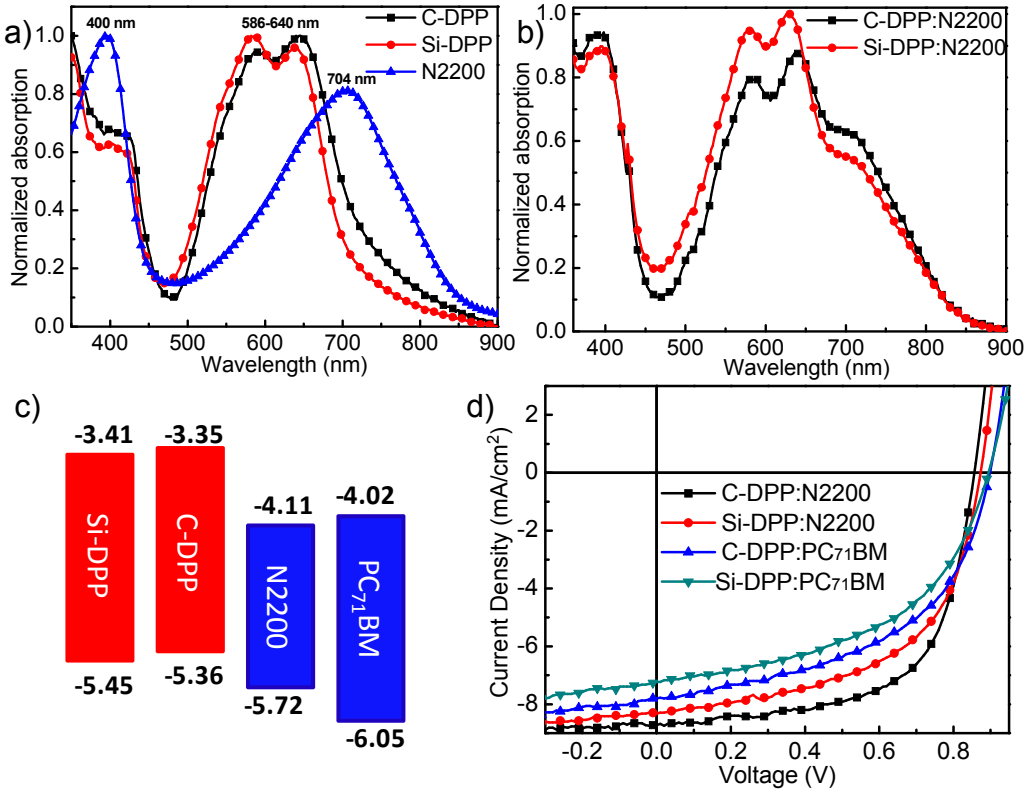

Fig. 2 a) UV-vis spectra of neat films of 3D-DPPs and N2200; b) UV-vis spectra of 3D-DPPs:N2200 BHJ films; c) FOE diagram of 3D-DPPs, N2200 and $PC_{71}BM$; d) *J-V* curves of the optimal solar cells of 3D-DPPs:N2200 and 3D-DPPs: $PC_{71}BM$.

Table 1 Photovoltaic Parameters of the Optimal Cells based on 3D-DPPs:N2200 and 3D-DPPs:$PC_{71}BM$ under the illumination of AM 1.5G, 100 mW cm^{-2}

D:A	V_{OC} [V]	J_{SC} [mA cm^{-2}]	*FF*	PCE [%][c]	Cal. J_{SC}[d] [mA cm^{-2}]	μ_h [10^{-4} cm^2 $V^{-1}s^{-1}$][e]	μ_e [10^{-4} cm^2 $V^{-1}s^{-1}$][e]	μ_h/μ_e
C-DPP:N2200[a]	0.87±0.01	8.59±0.18	0.62±0.01	4.64(4.45)	8.71	3.58	2.87	1.25
Si-DPP:N2200[a]	0.86±0.01	8.14±0.22	0.54±0.03	4.02(3.93)	8.21	2.12	0.89	2.34
C-DPP:$PC_{71}BM$[b]	0.89±0.01	7.69±0.14	0.50±0.01	3.56(3.41)	7.74	2.20	0.11	20
Si-DPP:$PC_{71}BM$[b]	0.89±0.01	7.12±0.14	0.49±0.01	3.22(3.12)	7.19	1.65	0.33	5

[a]The D:A ratio is 1:1 (w/w). [b]The D:A ratio is 1:1.5 (w/w). [c]The best and average (in brackets, over 20 devices) PCEs. [d]Calculated from IPCE; average values from 12 devices. [e]Hole and electron mobilities by SCLC method.

2.3 BHJ device performances

Inverted devices with the configuration of indium tin oxide (ITO)/ZnO/3D-DPPs:N2200/MoO_3/Ag were subsequently fabricated to investigate the performance of corresponding BHJ OPVs. The devices based on Si-DPP:N2200 (1:1) BHJ are first optimized with three sets of solvents: chloroform (CF), chlorobenzene (CB), and the mixed CF/CB (1:1, v/v). The PCEs of Si-DPP:N2200 (1:1) based devices processed by CF, CB and CF/CB were 1.03, 1.73 and 3.76%, respectively (Fig. S9 and Table S1). Note that the PCE of 3.76% in the Si-DPP:N2200 based device was accomplished without applying any post-treatments or additives. It is close to the highest PCE (3.9%) reported for molecular donor/polymer acceptor device using di-DPP:N2200 BHJ with 1-chloronaphthalene (CN) as additive.[26a] By adding 3% (v/v) CN, the PCE of **Si-DPP**:N2200 is further improved to 4.02%. Under the similar processing condition, **C-DPP**:N2200 exhibits the highest PCE of 4.64% (with open circuit voltage, V_{OC} of 0.86 V; short current, J_{SC} of 8.72 mA cm^{-2}, and fill factor, *FF* of 0.62). Fig. 2d shows the current density-voltage (*J-V*) characteristic curves of the optimal cells under the simulated AM 1.5 G irradiation with intensity of 100 $mWcm^{-2}$, and Table 1 summarizes the photovoltaic parameters.

The optimized 3D-DPPs:$PC_{71}BM$ devices were employed to compare with 3D-DPPs:N2200 devices. Unlike the 3D-DPPs:N2200, the desired solvent and effective additive for 3D-DPPs:$PC_{71}BM$ were CF and 1,8-diiodooctane (DIO, 3% v/v), respectively. The highest PCEs obtained for **Si-DPP**:$PC_{71}BM$ and **C-DPP**:$PC_{71}BM$ are 3.22% and 3.56%, respectively (Fig. 2d and Table 1), which are albeit lower than the N2200-based cells. The inferior PCEs of 3D-DPPs:$PC_{71}BM$ are mainly ascribed to their lower J_{SC} and *FF*. Although a large variety of star-shaped molecular donors have been developed for OPVs,[32-34] the highest PCE for PCBM-based OPVs using these donors remain around 5%.[34a,b] These molecular donor may not be able to form optimal nanoscale D-A phase separated morphology with $PC_{71}BM$ (ESI, Fig. S13a). However, the PCE (4.64%) achieved in our study without using fullerene is very close to the highest PCE of star-shaped donor:$PC_{71}BM$ BHJs reported so far,[34a,b] implying polymer acceptors have the potential to be further explored for pairing with the star-shaped or 3D-shaped molecular donors.

2.4 Photoluminescence (PL) and IPCE measurements

To better understand their photophysical properties, PL spectra of neat films (3D-DPPs, N2200, $PC_{71}BM$) and their corresponding D-A blends, in conjunction with the device IPCE spectra were studied. The PL of 1:1 blends show effective and mutual quenching of individual 3D-DPPs and N2200 emission, suggesting efficient charge transfer between3D-DPPs and N2200 (Fig. 3). However, the emission of **C-DPP** can be quenched more effectively by N2200 than that of **Si-DPP**, which may account for the higher *J*sc observed from **C-DPP**:N2200 BHJ OPVs (Fig. 3a and Table 1). Fig. 3b displays the corresponding IPCE spectra of solar cells based on **C-DPP**:N2200, **Si-DPP**:N2200, **C-DPP**:$PC_{71}BM$, and **Si-DPP**:$PC_{71}BM$. The calculated J_{SC}s from IPCE are 8.71, 8.21, 7.74, and 7.19 mA cm^{-2}, respectively (Table 1), which are consistent with the measured J_{SC} values. Interestingly, the IPCEs of 3D-DPPs:N2200 blends extend from 350 nm to 800 nm, which match well with their UV-vis absorption spectra (Fig. 3b). It indicates that light absorbed by both 3D-DPPs and N2200 are effectively converted into current in solar cells (Fig. S11), suggesting excitons generated from donor and acceptor domain can be dissociated effectively at the D-A junction.

The IPCE spectra of 3D-DPPs:$PC_{71}BM$ BHJs are ranging from 350-700 nm, which are slightly lower and narrower than those of 3D-DPPs:N2200. Aside from the weak absorption of $PC_{71}BM$ (Fig. S8, S12), the amorphous 3D-DPPs may intimately mix with $PC_{71}BM$ to prevent the formation of suitable nanoscale D-A phase separation. As shown by the DFT calculations, 3D-DPPs have a radius of more than 2.0 nm (Fig. 1). The spherical PCBM with a diameter of ~ 0.8 nm[34] would be embraced by 3D-DPPs, leading to intimate D-A mixing (Fig. S13a). Such an intimate D-A mixing will enhance quenching of PL emission (ESI, Fig. S14), however, it will adversely affect charge separation,[36] and decrease the IPCE of 3D-DPPs:$PC_{71}BM$ BHJs. Unlike fullerene-based BHJs, the blend of crystalline N2200[3b,25] with amorphous 3D-DPPs allows easier nanoscale phase separation (Fig. S13b), facilitating better charge separation and transport.

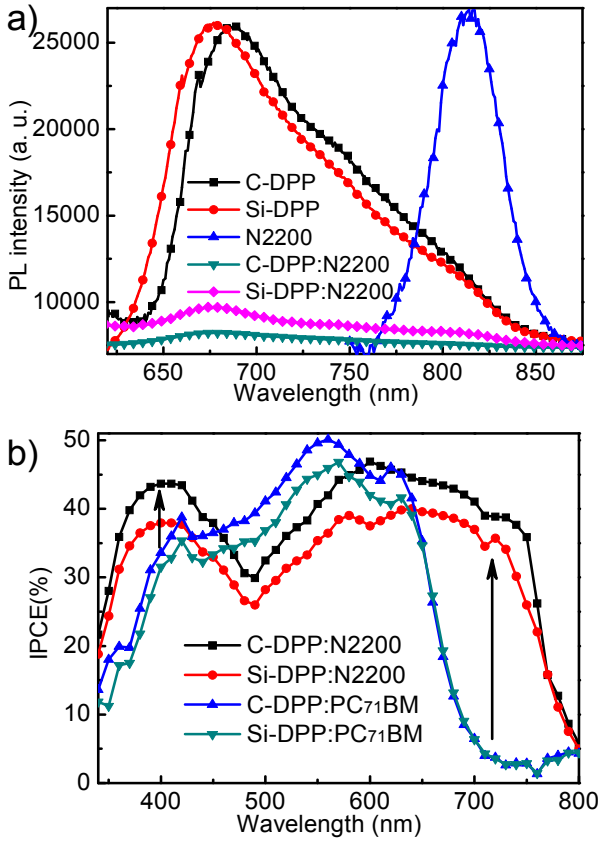

Fig. 3 a) Steady PL spectra of 3D-DPPs, N2200 neat films, and 3D-DPPs:N2200 BHJ films (1:1, w/w) (excited at 650 nm) b) IPCE spectra of 3D-DPPs:N2200 and 3D-DPPs:$PC_{71}BM$ BHJs.

2.5 BHJ morphology and charge carrier mobility

Atomic force microscopy (AFM) and space-charge-limited-current (SCLC) measurements were further employed to investigate surface morphology and charge mobility of the active layers. AFM scans were carried out for films spin-coated on ITO substrates. AFM images of the active layers based on 3D-DPPs:N2200 and 3D-DPPs:$PC_{71}BM$ are shown in Fig. S15. As compared to **Si-DPP**-based BHJs, **C-DPP**-based BHJs generally exhibit smoother surface (Fig. S15). For the SCLC tests, all devices were fabricated by using the identical procedure for solar cell preparation. The *J-V* curves for the hole-only and electron-only devices are shown in Fig. S16. The third-last and second-last columns in Table 1 list the corresponding values. The hole mobility (μ_h) of **C-DPP**:N2200, **Si-DPP**:N2200, **C-DPP**:$PC_{71}BM$ and **Si-DPP**:$PC_{71}BM$ BHJs are 3.58, 2.12, 2.20, and 1.65 ($\times 10^{-4}$cm^2 V^{-1} s^{-1}), respectively, and the corresponding electron mobility (μ_e) are 2.87, 0.89, 0.11, and 0.33 ($\times 10^{-4}$cm^2 V^{-1} s^{-1}), respectively. Among the four devices, **C-DPP**:N2200 exhibits the highest and the most balanced charge mobility with the μ_h/μ_e ratio of 1.25 (Table 1), compared with the more imbalanced μ_h/μ_e ratios of 2.3 for **Si-DPP**:N2200, 20.0 for C-DPP:$PC_{71}BM$, and 5.0 for **Si-DPP**:$PC_{71}BM$. This may explain the higher *FF* (0.62) obtained for **C-DPP**:N2200 based device.

Although electron mobility of 3D-DPPs:N2200 BHJs (~10^{-4} cm^2 V^{-1} s^{-1}) is one order of magnitude higher than those of 3D-DPPs:$PC_{71}BM$ BHJs (~10^{-5} cm^2 V^{-1} s^{-1}), the hole mobility of all four blends are very similar(~10^{-4} cm^2 V^{-1} s^{-1}) (Table 1). This suggests that the hole-transporting channels generated from 3D-DPPs are quite insensitive to mixing with either N2200 or $PC_{71}BM$, resulting in similar level of hole mobility. This coincides well with the findings of other 3D-shaped conjugated structures reported in the literature that also form uniform, amorphous thin films with isotropic properties.[30] On the other hand, the electron transport is more sensitive to electron acceptor used with polymer N2200 forming better nanoscale continuous networks than that of molecular fullerene when blended with 3D-DPPs.

2.6 General applicability

Usually, efficient OPV devices often consist of spherical shaped fullerenes as acceptor and linear polymer as donor, and the best performing non-fullerene acceptors are also non-planar or 3D-shaped.[4-23] The same rationale could also be applied here, with a BHJ composed of a **3D donor** and a **linear polymer acceptor** with one of the donor or acceptor[4-23] be non-planar or 3D-shaped instead of both 3D-shaped, to achieve high efficiency in devices.

To further assess the general applicability of 3D-donor/linear polymer acceptor combination, fluoro-substituted N2200 (di-F-N2200)[3b] was also used as another polymeric acceptor (ESI, Fig. S10) to pair with the 3D-DPP donors. The preliminary device results derived from the 3D-DPPs:di-F-N2200 BHJs also showed promising PCEs of 4.41% (**Si-DPP**:di-F-N2200) and 4.60% (**C-DPP**:di-F-N2200), respectively (data not shown), which supports the hypothesis of the effectiveness of 3D-donor:polymer acceptor blends.

3 Conclusions

In summary, two novel DPP-based 3D molecular donors were designed and facilely synthesized via an atom efficient direct C-H arylation reaction. The 3D-DPPs:N2200 BHJ non-fullerene based devices exhibit better performance than those derived from the fullerene-based ones, showing a respectable PCE of 4.64% for the 3D-DPPs:N2200, which is ~30% higher than that derived from the 3D-DPPs:$PC_{71}BM$. The superior performance is attributed to more efficient IPCE generated from the complementary light absorption of 3D-DPPs and N2200, and the high *FF*s obtained from the balanced charge mobilities. In contrast to the well-developed BHJs that consist of non-planar or **3D acceptors** and **polymer donors**,[4-23] the current work represents the first BHJ OPV based on **3D donors** and **polymer acceptors**. This preliminary yet promising result demonstrates the strategy of blending 3D-donors with linear polymer acceptors can be effective for achieving high-performance OPVs.

4 Experimental

4.1 Materials and methods

Unless otherwise specified, chemicals and solvents were purchased from Aldrich. All ^{1}H and ^{13}C NMR spectra were obtained in chloroform-*d*, with Bruker 300, and Bruker Avance DRX-499. ^{13}C NMR (126 MHz) spectra were measured with a proton-decoupling pulse program. Chemical shifts for ^{1}H and ^{13}C NMR were referenced to residual signals from $CDCl_3$ (^{1}H NMR δ =7.26 ppm and ^{13}C NMR δ =77.23 ppm). Matrix-assisted laser desorption-ionization time of flight mass spectrometry (MALDI-TOF MS) was performed on a Bruker Autoflex II. Samples were prepared by diluting the molecules in CH_2Cl_2 using 2,5-dihydroxybenzoicacid as the matrixes. Elemental analyses were conducted on a Flash EA 1112 elemental analyzer. Theoretical calculations based on density functional methods have been performed for 3D-DPPswith Gaussian09 program. Becke's three-parameter gradient-corrected functional (B3LYP) with 6-31G(d,p) basis was used to optimize the geometry.

DSC was measured on a WCT-2 thermal balance. UV−vis spectra were recorded with a Jasco V-670. PL spectra were measured on Fluoroskan Ascent FL. CV was done on a CHI 660C electrochemical workstation with Pt disk, Pt plate, and standard 10 calomel electrode (SCE) as working electrode, counter electrode, and reference electrode, respectively, in a 0.1 molL^{-1}tetrabutylammoniumhexafluorophosphate (Bu_4NPF_6) CH_2Cl_2 solution. The current-voltage (*J-V*) curves were measured with Keithley 2400 measurement source units at room temperature in air. The photocurrent was measured under a calibrated solar simulator (Abet 300 W) at 100 mW cm^{-2}.

The EQE system uses a lock-in amplifier (Stanford Research Systems SR830) to record the short circuit current under chopped monochromatic light. AFM images were obtained by a Nano ScopeIIIa (Digital instrument Inc.) operating in the tapping mode. SCLC were tested in electron-only devices with a configuration of ITO/ZnO/3D-DPPs:N2200 or $PC_{71}BM$/Ca (20 nm)/Al (130 nm) and hole-only devices with a configuration of ITO/PEDOT:PSS/3D-

DPPs:N2200 or $PC_{71}BM/MoO_3/Ag$. The devices were prepared using the above-mentioned procedure. In hole-only deices, PEDOT:PSS (Clevios-PVP AI 4083) was spin-coated on ITO substrates at 5000 rpm for 30 sec and then annealed at 140 ℃for 10 min. The mobilities were determined by fitting the dark current according to the following equation:

$$J(V) = \frac{9V^2}{8L^3}\varepsilon_0\varepsilon_r\mu_0 e^{\left(0.89\gamma\sqrt{V/L}\right)}$$

Where J is the dark current density (mA cm^{-2}), μ_0 is the zero-field mobility (cm^2/V sec), ε_0 is thepermittivity of free space ($88.54*10^{-12}$ mA sec/V sec), ε_r is the relative permittivity of the material (3), V is the effectie voltage ($V=V_{Applied}-V_{Built\text{-}in}-V_{seriesresistane}$), and L is the thickness of the active layer.

4.2 Synthetic procedures

The synthetic proceduresforprecursors TBPM, TBPS and Ph-DPP can be found in ESI.

Synthesis of ***C-DPP*** *and* ***Si-DPP***: The starting Ph-DPP (140 mg, 0.23 mmol), TBPM or TBPS (0.05 mmol, 31.8 mg and 32.6 mg for TBPM and TBPS, respectively), anhydrous K_2CO_3 (55 mg, 0.4 mmol), pivalic acid (PivOH, 6.1 mg, 0.06 mmol), $Pd(OAc)_2$ (2.3 mg, 0.01 mmol) were stirred in anhydrous dimethylacetamide (DMAc, 5 mL) for 24 h at 105 °C under argon in a Schlenk tube. After cooling to room temperature, the mixture was poured into a 250 mL NaCl aqueous solution to remove salts and high boiling point solvent (DMAc). The precipitate was extracted with $CHCl_3$ (3×20 mL). The combined organic layers was washed with distilled water and dried over anhydrous Na_2SO_4. Removal of $CHCl_3$ by a rotary evaporator afforded the crude products, which were then purified by column chromatography on silica gel using the mixture of CH_2Cl_2 and hexane as eluent (6:1, v/v) and gave the products. Both **C-DPP** (139 mg, yield 90%) and **Si-DPP** (145 mg, yield 94%) as dark blue solids.

C-DPP: ^{1}H NMR (300 MHz, $CDCl_3$) δ 8.99 (dd, J = 7.1, 4.2 Hz, 8H), 7.67 (t, J = 8.0 Hz, 16H), 7.52 –7.31 (m, 28H), 4.09 (d, J = 7.4 Hz, 16H), 1.96 (s, 8H), 1.33 (d, J = 33.1 Hz, 64H), 0.98 – 0.82 (m, 48H); ^{13}C NMR (126 MHz, $CDCl_3$, δ): 161.75, 150.04, 148.79, 146.65, 140.00, 139.73, 136.91, 133.19, 131.57, 129.18, 129.03, 128.83, 126.15, 125.67, 124.71, 124.51, 108.60, 46.09, 39.15, 30.35, 28.47, 23.69, 23.17, 14.13, 10.61; MALDI-TOF MS m/z: $[M]^+$ calcd for $C_{169}H_{188}N_8O_8S_8$, 2715.89; found, 2716.12; elemental analysis: calcd: C, 74.74; H, 6.98; N, 4.13%. Found: C, 74.54; H, 7.00; N, 4.12%.

Si-DPP: ^{1}H NMR (300 MHz, $CDCl_3$) δ 9.00 (s, 8H), 7.74 (dd, J = 20.0, 8.5 Hz, 24H), 7.56 (d, J = 3.3 Hz, 4H), 7.47 (d, J = 7.7 Hz, 16H), 4.11 (d, J = 7.4 Hz, 16H), 1.97 (s, 8H), 1.34 (d, J = 35.4 Hz, 64H), 0.97 – 0.85 (m, 48H). ^{13}C NMR (126 MHz, $CDCl_3$, δ): 161.62, 149.86, 148.93, 140.23, 139.55, 137.06, 136.97, 134.75, 133.91, 133.16, 129.23, 126.13, 125.63, 124.96, 124.53, 108.38, 108.20, 99.97, 46.01, 39.29, 30.43, 28.58, 23.69, 23.11, 14.09, 10.59; MALDI-TOF MS m/z: $[M]^+$ calcd for $C_{168}H_{188}N_8O_8S_8Si$, 2731.97; found, 2732.09; elemental analysis: calcd: C, 73.86; H, 6.94; N, 4.10%. Found: C, 73.74; H, 6.92; N, 4.11%.

4.3 Device fabrication

Solar cell devices were fabricated with an inverted structure of ITO/ZnO (30 nm)/active layer (90−100 nm)/MoO_3 (8 nm)/Ag (120 nm). The ITO-coated glass was cleaned in an ultrasonic bath of acetone and isopropanol, and treated in ultraviolet-ozone chamber for 30 min. A ZnO precursor solution was spin-coated onto pre-cleaned ITO glass substrates at 4000 rpm for 60 s and then annealed at 200 °C for 1 h in air to complete the thin layer of ZnO (ca. 30 nm).The ZnO precursor solution was prepared by dissolving zinc acetate dehydrate $C_4H_6O_4Zn{\cdot}2(H_2O)$ (99.5%, Merck1 g) and monoethanolamine ($HOCH_2CH_2NH_2$, 98% Acros, 0.28 g) in2-methoxyethanol ($CH_3OCH_2CH_2OH$, Aldrich, 98%, 10 mL) under stirring for 8 h for hydrolysis reaction and aging.The active layer was spin-coated from the blend solution (30 mg/mL for 3D-DPPs:N2200, and 15 mg/mL for 3D-DPP:$PC_{71}BM$). After spin-coating, the films were placed in a closed jar for slow drying of solvent. Finally, MoO_3 and Ag were thermally evaporated as anode electrode at a pressure of < 10^{-7} torr. The active area of each device was 3.14 mm^2 defined by a shadow mask which was cut by laser beam technique. All masked tests gave consistent results with relative errors within 1%. The photovoltaic performance was measured under nitrogen inside a glove box. The current density-voltage (J-V) characteristics were measured with a Keithley2400 source-meter under AM 1.5 G (100 $mWcm^{-2}$) illumination which was accurately calibrated employing a standard Si photodiode detector equipped with a KG-5 filter, which can be traced back to the standard cell of the National Renewable Energy Laboratory (NREL). Devices were measured with shadow masking. The AM 1.5 G illumination was simulated by using an Oriel 300 W Solar Simulator. The solar cell devices were fabricated and measured over 20 devices for reliability of the device performance.

Acknowledgements

The authors acknowledge the Asian Office of Aerospace R&D (FA2386-11-1-4072), the Office of Naval Research (N00014-1-0170), the National Natural Science Foundation of China (21244008, 21374075 and 51473142), and the China Scholarship Council (201308330072) for financial support. The authors thank Dr. Jun-Yong Wu for molecular geometry optimization.

Notes and references

1 (*a*) J. Y. Kim, K. Lee, N. E. Coates, D. Moses, T.-Q. Nguyen, M. Dante and A. J. Heeger, *Science*, 2007, **317**, 222; (*b*) M. Hösel, D. Angmo, R. R. Søndergaard, G. A. dos R. Benatto, J. E. Carlé, M. Jørgensen and F. C. Krebs, *Adv. Sci.*, 2014, **1**, 1400002; (*c*) P. Cheng, H. Bai, N. K. Zawacka, T. R. Andersen, W. Liu, E. Bundgaard, M. Jørgensen, H. Chen, F. C. Krebs and X. Zhan, *Adv. Sci.*, 2015, **2**, 1500096.

2 (*a*) Y. Lin and X. Zhan, *Mater. Horiz.*, 2014, **1,** 470; (*b*) A. F. Eftaiha, J.-P. Sun, I. G. Hill and G. C. Welch, *J. Mater. Chem. A*, 2014, **2**, 1201; (*c*) S. M. McAfee, J. M. Topple, I. G. Hill

and G. C. Welch, *J. Mater. Chem. A*, 2015, **3**, 16393; (*d*) A, Facchetti, *Mater. Today*, 2013, **16**, 123.

3 (*a*) Y. Lin, Z.-G. Zhang, H. Bai, J. Wang, Y. Yao, Y. Li, D. Zhu and X. Zhan, *Energy Environ. Sci.*, 2015, **8**, 610; (*b*) Y. Lin, J. Wang, Z.-G. Zhang, H. Bai , Y. Li , D. Zhu and X. Zhan, *Adv. Mater.*, 2015, **27**, 1170; (*c*) J. W. Jung, J. W. Jo, C.-C. Chueh, F. Liu, W. H. Jo, T. P. Russell and A. K.-Y. Jen, *Adv. Mater.*, 2015, **27**, 3310; (d) Y.-J. Hwang, B. A. E. Courtright, A. S. Ferreira, S. H. Tolbert, S. A. Jenekhe, *Adv. Mater.*, 2015, **27**, 4578.

4 (*a*) J. Zhao, Y. Li, H. Lin, Y. Liu, K. Jiang, C. Mu, T. Ma, J. Y. L. Lai and H. Yan, *Energy Environ. Sci.*, 2015, **8**, 520; (*b*) H. Li, Y.-J. Hwang, B. A. E. Courtright, F. N. Eberle, S. Subramaniyan and S. A. Jenekhe, *Adv. Mater.*, 2015, **27**, 3266.

5 Y. Zang, C.-Z. Li, C.-C. Chueh, S. T. Williams, W. Jiang, Z.-H. Wang, J.-S. Yu and A. K.-Y. Jen, *Adv. Mater.*, 2014, **26**, 5708.

6 Y. Zhong, M. T. Trinh, R. Chen, W. Wang, P. P. Khlyabich, B. Kumar, Q. Xu, C.-Y. Nam, M. Y. Sfeir, C. Black, M. L. Steigerwald, Y.-L. Loo, S. Xiao, F. Ng, X.-Y. Zhu and C. Nuckolls, *J. Am. Chem. Soc.*, 2014, **136**, 15215.

7 W. Jiang, L. Ye, X. Li, C. Xiao, F. Tan, W. Zhao, J. Hou and Z. Wang, *Chem. Commun.*, 2014, **50**, 1024.

8 (*a*) H. Shi, W. Fu, M. Shi, J. Ling and H. Chen, *J. Mater. Chem. A*, 2015, **3**, 1902; (*b*) Y. Yang, G. Zhang, C. Yu, C. He, J. Wang, X. Chen, J. Yao, Z. Liu and D. Zhang, *Chem. Commun.*, 2014, **50**, 9939.

9 (*a*) X. Zhang, Z. Lu, L. Ye, C. Zhan, J. Hou, S. Zhang, B. Jiang, Y. Zhao, J. Huang, S. Zhang, Y. Liu, Q. Shi, Y. Liu and J. Yao, *Adv. Mater.*, 2013, **25**, 5791; (*b*) Y. Lin, J. Wang, S. Dai, Y. Li, D. Zhu and X. Zhan, *Adv. Energy Mater.*, 2014, **4**, 1400420.

10 Q. Yan, Y. Zhou, Y.-Q. Zheng, J. Pei and D. Zhao, *Chem. Sci.*, 2013, **4**, 4389.

11 Z. Lu, B. Jiang, X. Zhang, A. Tang, L. Chen, C. Zhan and J. Yao, *Chem. Mater.*, 2014, **26**, 2907.

12 S. Rajaram, R. Shivanna, S. K. Kandappa and K. S. Narayan, *J. Phys. Chem. Lett.*, 2012, **3**, 2405.

13 R. Shivanna, S. Shoaee, S. Dimitrov, S. K. Kandappa, S. Rajaram, J. R. Durrant and K. S. Narayan, *Energy Environ. Sci.*, 2014, **7**, 435.

14 Y. Lin, Y. Wang, J. Wang, J. Hou, Y. Li, D. Zhu, X. Zhan, *Adv. Mater.* **2014**, *26*, 5137.

15 Y. Liu, J. Y. L. Lai, S. Chen, Y. Li, K. Jiang, J. Zhao, Z. Li, H. Hu, T. Ma, H. Lin, J. Liu, J. Zhang, F. Huang, D. Yu and He Yan, *J. Mater. Chem. A*, 2015, **3**, 13632.

16 Y.-Q. Zheng, Y.-Z. Dai, Y. Zhou, J.-Y. Wang and J. Pei, *Chem. Commun.*, 2014, **50**, 1591.

17 W. Chen, X. Yang, G. Long, X.Wan, Y. Chen and Q. Zhang, *J. Mater. Chem. C*, 2015, **3**, 4698.

18 D. Xia, D. Gehrig, X. Guo, M. Baumgarten, F. Laquai and K. Müllen, *J. Mater. Chem. A*, 2015, **3**, 11086.

19 Y. Cai, L. Huo, X. Sun, D. Wei, M. Tang and Y. Sun, *Adv. Energy Mater.*, 2015, **5**, 1500032.

20 Z. Mao, W. Senevirathna, J.-Y. Liao, J. Gu, S. V. Kesava, C. Guo, E. D. Gomez and G. Sauvé, *Adv. Mater.*, 2014, **26**, 6290.

21 Y. Liu, C. Mu, K. Jiang, J. Zhao, Y. Li, L. Zhang, Z. Li, J. Y. L. Lai, H. Hu, T. Ma, R. Hu, D. Yu, X. Huang, B. Z. Tang and H. Yan, *Adv. Mater.*, 2015, **27**, 1015.

22 S.-Y. Liu, C.-H. Wu, C.-Z. Li, S.-Q. Liu, K.-H. Wei, H.-Z. Chen and A. K.-Y. Jen, *Adv. Sci.*, 2015, **2**, 1500014.

23 H. Li, T. Earmme, G. Ren, A. Saeki, S. Yoshikawa, N. M. Murari, S. Subramaniyan, M. J. Crane, S. Seki and S. A. Jenekhe, *J. Am. Chem. Soc.,* 2014, **136**, 14589.

24 B. A. Gregg, *J. Phys. Chem. Lett.*, 2011, **2**, 3013.

25 (*a*) H. Yan, Z. Chen, Y. Zheng, C. Newman, J. R. Quinn, F. Dötz, M. Kastler and A. Facchetti, *Nature*, 2009, **457**, 679; (*b*) C. Mu, P. Liu, W.Ma, K. Jiang, J. Zhao, K. Zhang, Z. Chen, Z. Wei, Y. Yi, J. Wang, S.Yang, F. Huang, A. Facchetti, H. Ade and H. Yan, *Adv. Mater.*, 2014, **26**, 7224.

26 (*a*) Z. Tang, B. Liu, A. Melianas, J. Bergqvist, W. Tress, Q. Bao, D. Qian, O. Inganäs and F. Zhang, *Adv. Mater.*, 2015, **27**, 1900; (*b*) Z. Li, J. D. A. Lin, H. Phan, A. Sharenko, C. M. Proctor, P. Zalar, Z. Chen, A. Facchetti and T.-Q. Nguyen, *Adv. Funct. Mater.*, 2014, **24**, 6989; (*c*) Y. J. Kim, D. S. Chung and C. E. Park, *Nano Energy*, 2015, **15**, 343; (*d*) J. Yuan and W. Ma, *J. Mater. Chem. A*, 2015, **3**, 7077; (*e*) D. Mori, H. Benten, I. Okada, H. Ohkita and S. Ito, *Energy Environ. Sci.*, 2014, **7**, 2939; (*f*) T. Earmme, Y.-J. Hwang, N. M. Murari, S. Subramaniyan and S. A. Jenekhe, *J. Am. Chem. Soc.*, 2013, **135**, 14960; (*g*) H. Kang, M. A. Uddin, C. Lee, K.-H. Kim, T. L. Nguyen, W. Lee, Y. Li, C. Wang, H. Y. Woo and B. J. Kim, *J. Am. Chem. Soc.*, 2015, **137**, 2359.

27 (*a*) Y. Wang, X. Zhao and X. Zhan, *J. Mater. Chem. C*, 2015, **3**, 447; (*b*) P. Cheng, X. Zhao, W. Zhou, J. Hou, Y. Li and X. Zhan, *Org. Electron.*, 2014, **15**, 2270.

28 (*a*) F. Grenier, B. R. Aich, Y. Lai, A. B. Holmes, Y. Tao, W. W. H. Wong and M. Leclerc, *Chem. Mater.*, 2015, **27**, 2137; (*b*) W. Liu, S. Liu, N. K. Zawacka, T. R. Andersen, P. Cheng, L. Fu, M. Chen, W. Fu, E. Bundgaard, M. Jørgensen, X. Zhan, F. C. Krebs and H. Chen, *J. Mater. Chem. A*, 2014, **2**, 19809.

29 (*a*) S.-Y. Liu, M.-M. Shi, J.-C. Huang, Z.-N. Jin, X.-L. Hu, H.-Y. Li, A. K.-Y. Jen and H.-Z. Chen, *J. Mater. Chem. A*, 2013, **1**, 2795; (*b*) S.-Y. Liu, W.-Q. Liu, J.-Q. Xu, C.-C. Fan, W.-F. Fu, J. Ling, J.-Y. Wu, M.-M. Shi, A. K.-Y. Jen and H.-Z. Chen, *ACS Appl. Mater. Interfaces*, 2014, **6**, 6765; (*c*) S.-Y. Liu, W.-F. Fu, J.-Q. Xu, C.-C. Fan, H. Jiang, M.-M. Shi, H.-Y. Li, J.-W. Chen, Y. Cao and H.-Z. Chen, *Nanotechnology*, 2014, **25**, 014006.

30 Y. Shirota, *J. Mater. Chem.* **2005**, *15*, 75.

31 C. M. Cardona, W. Li, A. E. Kaifer, D. Stockdale and G. C. Bazan, *Adv. Mater.*, 2011, **23**, 2367.

32 Reviews about star-shaped molecules for OPVs, see: (*a*) A. L. Kanibolotsky, I. F. Perepichka and P. J. Skabara, *Chem. Soc. Rev.*, 2010, **39**, 2695; (*b*) J. Roncali, *Acc. Chem. Res.*, 2009, **19**, 1719; (*c*) J. Roncali, P. Leriche and A. Cravino, *Adv. Mater.*, 2007, **19**, 2045; (*d*) P. J. Skabara, J.-B. Arlin and Y. H. Geerts, *Adv. Mater.*, 2013, **25**, 1948; (*e*) T. Jarosz, M. Lapkowski and P. Ledwon, *Macromol. Rapid Commun.*, 2014, **35**, 1006; (*f*) S. A. Ponomarenko, Y. N. Luponosov, J. Min, A. N. Solodukhin, N. M. Surin, M. A. Shcherbina, S. N. Chvalun, T. Americ and C. Brabec, *Faraday Discuss.*, 2014, **174**, 313.

33 O. V. Kozlov, Y. N. Luponosov, S. A. Ponomarenko, N. K.-Busies, D. Y. Paraschuk, Y. Olivier, D. Beljonne, J. Cornil and M. S. Pshenichnikov, *Adv. Energy Mater*., 2014, **4**, 1401657.

34 (*a*) N. Cho, S. Paek, J. Jeon, K. Song, . D. Sharma and J. Ko, *J. Mater. Chem. A*, 2014, **2**, 12368; (*b*) J. Min, Y. N. Luponosov, A. Gerl, M. S. Polinskaya, S. M. Peregudova, P. V. Dmitryakov, A. V. Bakirov, M. A. Shcherbina, S. N. Chvalun, S. Grigorian, N. Kaush-Busies, S. A. Ponomarenko, T. Ameri and C. J. Brabec, *Adv. Energy Mater.*, 2014, **4**, 1301234; (*c*) H. X. Shang, H. J. Fan, Y. Liu, W. P. Hu, Y. F. Li and X. W. Zhan, *Adv. Mater.*, 2011, **23**, 1554.

35 A. Goel, J. B. Howard and J. B. V. Sande, *Carbon*, 2004, **42**, 1907.

36 W. Nie, G. Gupta, B. K. Crone, F. Liu, D. L. Smith, P. P. Ruden, C.-Y. Kuo, H.Tsai, H.-L. Wang, H. Li, S. Tretiak and A. D. Mohite, *Adv. Sci.*, 2015, **2**, 1500024.

The graphical and textual abstract for the Table of contents entry:

Three-dimensional molecular donors combined with polymeric acceptors for high performance fullerene-free organic photovoltaics

Shi-Yong Liu, Jae Woong Jung, Chang-Zhi Li, Jiang Huang, Jianyuan Zhang, Hongzheng Chen* and Alex K.-Y. Jen*

Two novel diketopyrrolopyrrole-based 3D electron donors have been synthesized via direct arylation. The fullerene-free organic photovoltaics (OPVs) based on the 3D-molecular donor:polymer acceptor showed a respectable power conversion efficiency of 4.64%, which outperforms OPVs derived from $PC_{71}BM$.